Internal Flow and Stability of Balance Piston for a Rocket Pump

Norio Kimura[1]*, Yuki Yoshii[1], Kengo Uchiyama[1], Kazuyoshi Miyagawa[1]

ISROMAC 2016

International Symposium on Transport Phenomena and Dynamics of Rotating Machinery

Hawaii, Honolulu

April 10-15, 2016

Abstract

In centrifugal pumps, axial thrust balancing is an important factor for stable operation. In particular, in rocket pumps, the stability of rotor assembly is very important to realize reliable high-pressure fluid delivery. Although balance piston, which is one of the self-compensating axial thrust balancing systems, was often used, there are sometimes axial vibration problems on the rotor. In this study, we examine static and dynamic characteristics of balance piston by performing experiments, computational fluid dynamics (CFD), and one-dimensional (1D) simulations, and we calculate parameters such as the static pressure in balance piston chamber and flowrate, orifice flow coefficient, phase difference from the rotor axial displacement to the static pressure fluctuation in the balance piston chamber. The results confirm that the experimental results can be predicted to some degree by performing simulations. Especially, it is found that the CFD simulation can be used to effectively predict the stability of balance piston..

Keywords

Rocket turbopump — Balance Piston —Dynamic characteristics

[1]*Department of Applied Mechanics and Aerospace Engineering, WASEDA University, Tokyo, Japan*

***Corresponding author**: t-a-50532@akane.waseda.jp

INTRODUCTION

Rocket pumps, which deliver liquid propellants to an engine combustion chamber, are required to achieve higher delivery pressure and higher rotational speed than industrial pumps; this enable them to achieve light-weight and good performance. These usually cause the operations to be carried out in very severe conditions. Therefore, a large axial thrust is often generated on the rotor. To balance the rotor axial force automatically, a balance piston, which is one of the axial thrust balancing systems is often applied, as shown in Fig. 1.

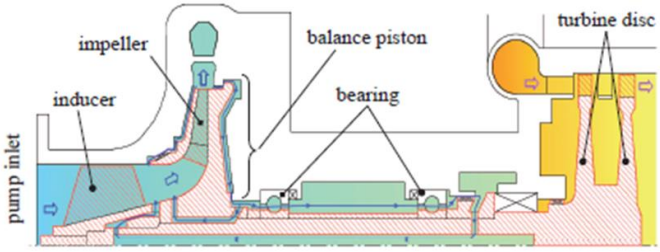

Fig. 1 Rocket LH2 turbopump with balance piston [1]

A balance piston is located in the back shroud of the main impeller. It is made by the edges of the casing wall and impeller shroud, and consists of the No. 1 orifice, which is located at the impeller outlet, No. 2 orifice, which is located at the small-radius position of the back shroud and the balance piston chamber, which is located between both orifices. Moreover, the rotor assembly with the balance piston can move in the axial direction within the orifices' clearance restriction, and stops at the balancing point of the pressure field around the balance piston.

If a rotor assembly moves in the axial direction from the pump inlet side toward the turbine side by the unbalanced axial thrust force imposed on the rotor, the No. 1 orifice clearance increases and the No. 2 orifice clearance decreases. As a result, the pressure in the balance piston chamber increases and the axial fluid force on the rotor back shroud also increases. Therefore, the rotor assembly moves back in the direction from the turbine side toward the pump-inlet side. Conversely, if a rotor assembly moves in the axial direction from the turbine side toward the pump-inlet side, the No. 1 orifice clearance decreases and the No. 2 orifice clearance increases. As a result, the pressure in the balance piston chamber decreases, and the axial fluid force on the rotor back shroud also decreases. Therefore, the rotor assembly moves back in the direction from the pump-inlet side toward the turbine side.

In this way, the balance piston has a self-balancing ability and keeps the rotor axial position stable in the static condition. However, because of the very severe operating conditions of a rocket turbopump, critical vibrations in the axial direction sometimes occur in the rotor assembly even though it is equipped with balance piston.

In these circumstances, we performed studies on a balance piston and impeller back shroud flow have been conducted to determine their characteristics. The analysis of the axial vibration caused by pump-impeller-

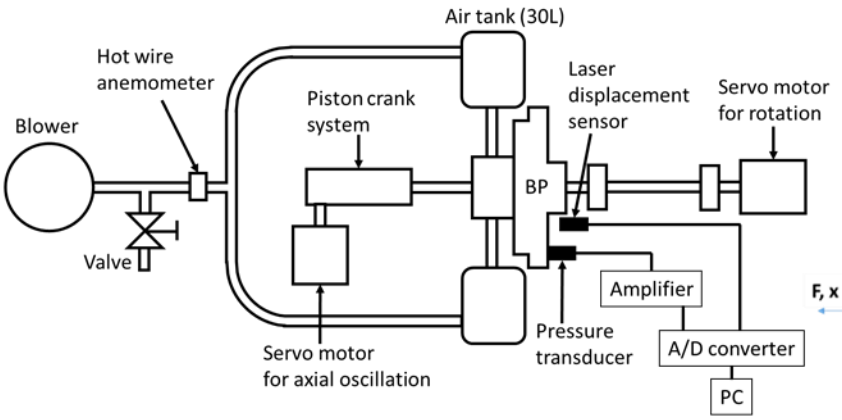

Fig. 2 Front view of the experimental setup

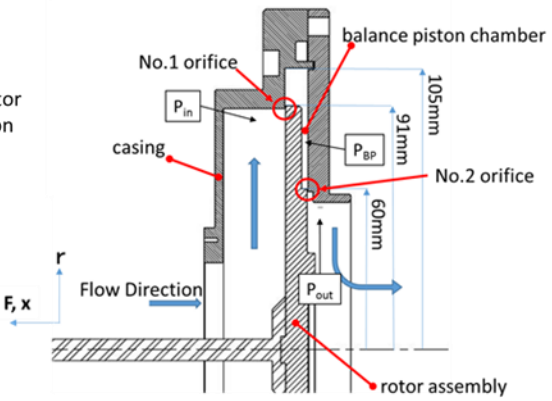

Fig. 3 Cross section of the test section

shroud forces was studied using bulk-flow model [2], and the dynamic characteristics of the radial-clearance flow between the axially oscillating rotating disk and stationary disk were investigated experimentally and using bulk-flow model [3]. The static characteristics of balance piston was examined [4], and the effects of the balance hole, grooves, and rotational speed on the balance piston's balancing capacity were determined by performing experiments and simulations. The dynamic characteristics of the balance piston was studied [1, 5, 6, 7], and its dynamic response and stability were examined by various methods such as eigen values, bode diagrams and unsteady response of one-dimensional (1D) simulations and unsteady computational fluid dynamics (CFD) simulations. From these studies, important factors that affect the balance piston stability have been better understood.

However, to the best of our knowledge, there have been no experimental studies of the dynamic characteristics of balance piston. To ensure the rocket-pump reliability, it is necessary to compare experimental and computational analyses in order to verify the validity of simulations, and to predict the detailed behavior of balance piston. To achieve these objectives, we performed experiments in air, CFD and 1D simulations to examine the internal flow of balance piston which affects the pump stability.

.

1. METHODS

Although working fluids of rocket turbopumps are usually liquid (liquid hydrogen, liquid oxygen, etc.), in this study, we conducted an air test of the balance piston as follows. Then, we carried out CFD and 1D simulations to predict and verify the characteristics of the balance piston.

1.1. Experiment

We performed the experimental investigation using the balance piston test equipment, as shown in Fig. 2. Then, Fig. 3 shows the balance piston cross section of the test section. The working fluid is air at normal temperature. The rotor assembly can move in the axial direction in order to adjust the clearance of the No. 1 and No. 2 orifices. The rotor assembly can to be oscillated axially by rotating the motor and piston-crank system. The axial oscillation sine waveform is shown in Eq. (1).

$$X = A_x \sin(\Omega t) \qquad (1)$$

The total clearance of the No. 1 and No. 2 orifices $x_1 + x_2$ is 0.7 mm, and the rotor-oscillating amplitude A_x is about 0.06 mm ($A_x/(x_1 + x_2) \fallingdotseq 0.0857$). The No. 1 orifice nominal clearance was $x_1/(x_1 + x_2)$=0.5. Further, the rotational speed N can vary by up to 2000 rpm. High-pressure air is supplied to the balance piston by using an air blower, and the supply pressure P_{in} can be adjusted using the valve. The effect of the rotational speed and supply pressure to the balance piston can be investigated using the above-mentioned test equipment. We measured the fluctuation in the static pressure using semiconductor pressure transducers (JTEKT PD-104K-10K), and the signals from the pressure transducer were amplified using amplifiers (JTEKT AA 6210). The measuring points is upstream the No. 1 orifice (P_{in}), downstream the No. 2 orifice (P_{out}) and the stationary chamber surface of the balance piston (P_{BP}). We measured the flowrate upstream of the balance piston using a hot-wire anemometer. We measured the axial displacement of the rotor using an inductive displacement sensor (KEYENCE EX-110V).

To investigate the effect of the No. 1 orifice's upstream pressure and the rotational speed on the balance piston characteristics, we used the test condition is (p_1, ω) = (4.69, 0), (4.69, ω_0), (14.07, 0).

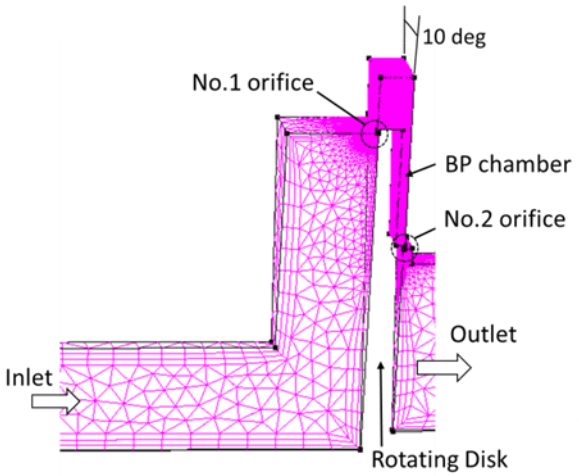

Fig. 4 CFD simulation numerical grid

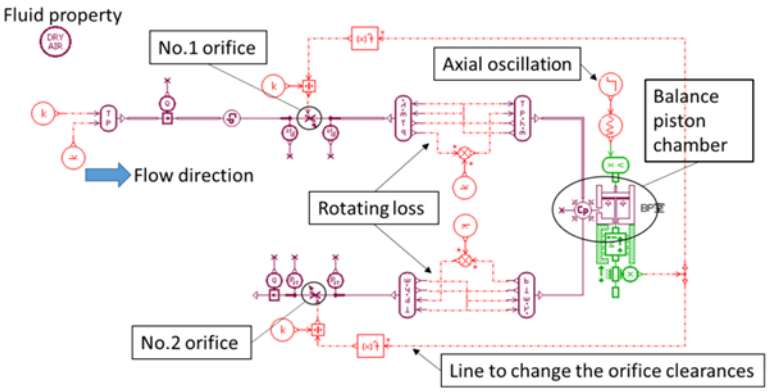

Fig. 5 1D simulation (AMESim) model

1.2 CFD Simulation

For comparison with the experiment results, and to investigate the internal flow of the balance piston, we performed CFD simulations. The simulation range and numerical grids are shown in Fig. 4. The number of cells was about 6,900,000, using a 10 [deg] periodic boundary condition circumferentially. The boundary condition at the inlet was the total pressure, and that at the outlet was the static pressure (atmospheric pressure). The working fluid was air in an incompressible condition. In this simulation, we used industrial code for fluid dynamics, Scryu/Tetra [8].

In the static characteristic simulation, the turbulence model was SST k-ω. In addition, we used five types of grid ($x_1/(x_1+x_2)$=0.214, 0.357, 0.5, 0.643, 0.786) to compare the effect of the difference in the clearance of the No. 1 orifice. In the dynamic characteristic simulation, we applied a large eddy simulation (LES) to consider the exact behavior of eddies in the balance piston chamber.

1.3. 1D Simulation

Fig. 5 shows the 1D simulation model that was developed using 1D multi-domain simulation code, AMESim [9]. When modeling the balance piston equipment, we combined pneumatic components (orifice, volume, pipe, and pressure-loss components, etc.) and mechanical components (pistons, rotors and oscillation generator components, etc.) and they were set to have the same boundary condition as in the experiment.

The pipe model includes the fluid compressibility and friction loss. In addition, we used Eq. (2) to model the rotating loss in the balance piston chamber that was caused by the rotating disk ΔP. It is assumed that the swirl ratio α is 0.5, which is the widely used value in clearance flow analysis [4].

$$\Delta P = \frac{1}{2}\rho(\alpha R_1\omega)^2 - \frac{1}{2}\rho(\alpha R_2\omega)^2 \qquad (2)$$

We applied the No. 1 and No. 2 orifice flow coefficients, which were determined by static experiments, and we simulated the dynamic response of the balance piston. Fig. 6 shows the No. 1 and No. 2 orifice flow coefficient C_{d1}, respectively. Although the plots have variations, the average orifice flow coefficients obtained by the experimental data are C_{d1} = 0.704, and C_{d2} = 0.790. These values were used in the 1D simulation to calculate the static and dynamic characteristics.

2. RESULTS AND DISCUSSION

2.1. Static Characteristics

Fig. 7(a) shows the static characteristics of the static pressure in the balance piston chamber. The horizontal axis is a nondimensional No. 1 orifice clearance $x_1/(x_1+x_2)$, and the vertical axis is a nondimensional static pressure in the balance piston p_{BP}. As the No. 1 orifice clearance increases, the pressure loss of the No. 1 orifice decreases and that of the No. 2 orifice increases; then, the static pressure in the balance piston chamber increases. We observed that the static-pressure curve obtained in the experiment, CFD, and 1D simulation result have almost the same characteristics.

The slope of the static pressure curve indicates the stiffness of the fluid in the balance piston chamber. We found that when about $x_1/(x_1+x_2)$ = 0.4, the stiffness is the largest. The slope of p_{in} = 14.07 is greater than that of p_{in} = 4.69. The results shows that as upstream pressure p_{in} of the No. 1 orifice increases, the stiffness of the balance piston increases. On the other hand, we observed no difference between the static-pressure curve and the stiffness of the balance piston for the

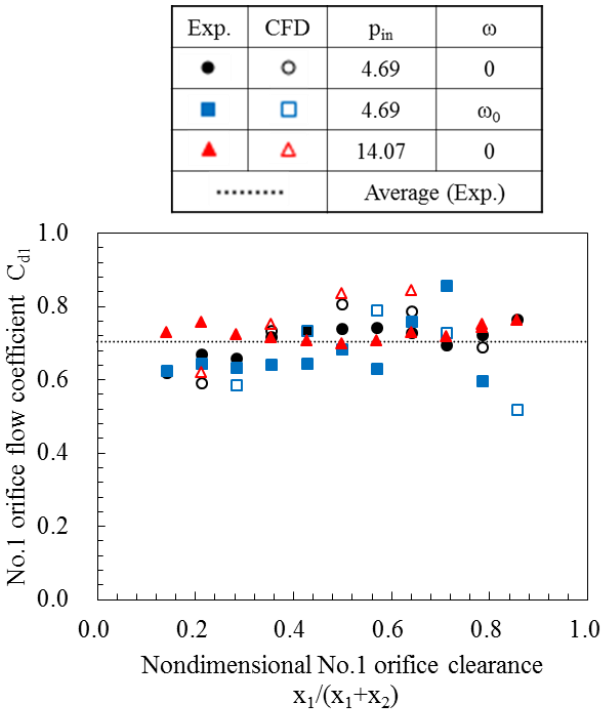

(a) No.1 orifice

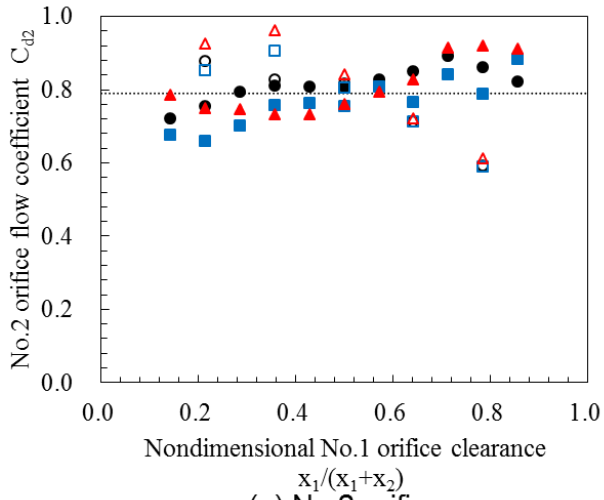

(a) No.2 orifice

Fig. 6 The orifice flow coefficient

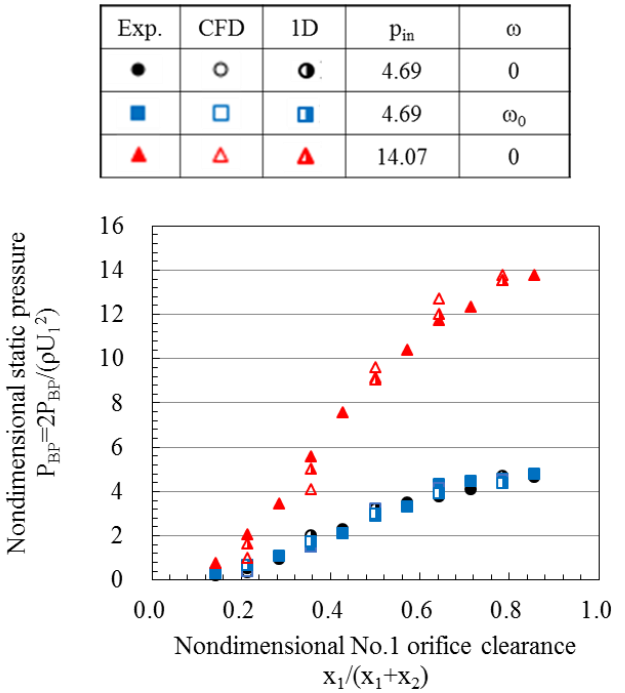

(a) Static pressure in BP chamber

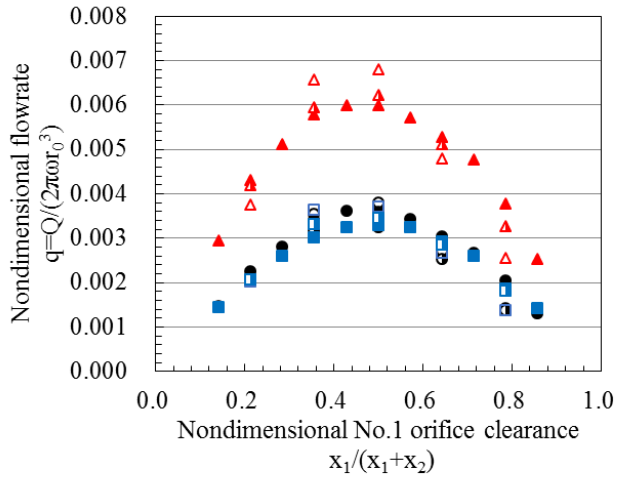

(b) Flowrate

Fig. 7 The static characteristics

$\omega = \omega_0$ and ω = 0 curves.

Fig. 7(b) shows the static characteristics of the flowrate. The horizontal axis represents the nondimensional clearance of the No. 1 orifice $x_1/(x_1 + x_2)$, and the vertical axis represents the nondimensional flowrate q. The flowrate increases up to the point where the total resistance of the No. 1 and No. 2 orifices is a minimum. Beyond that point, the flowrate decreases because the resistance of the No. 2 orifice increases. We obtained the flowrate curve obtained by the experiment, CFD, and 1D simulation results for almost the same characteristics. Then, when $x_1/(x_1 + x_2)$ = 0.5, the flowrate is a maximum and the total resistance of the No. 1 and No. 2 orifices is a minimum. As the upstream pressure of the No. 1 orifice increases, the differential pressure of the orifices increases, and the flowrate then increases. Similar to the static-pressure curve, the effect of the upstream pressure on the No. 1 is clearly shown in the figure, but the effect of the rotational speed ω could not be confirmed.

2.2 Dynamic characteristics

To clarify the factors that affect the balance piston stability, we discussed the effect of the two factors (rotational speed and upstream pressure of the No. 1 orifice) on the balance piston dynamic characteristics as follows.

To evaluate the balance piston stability, we used fast

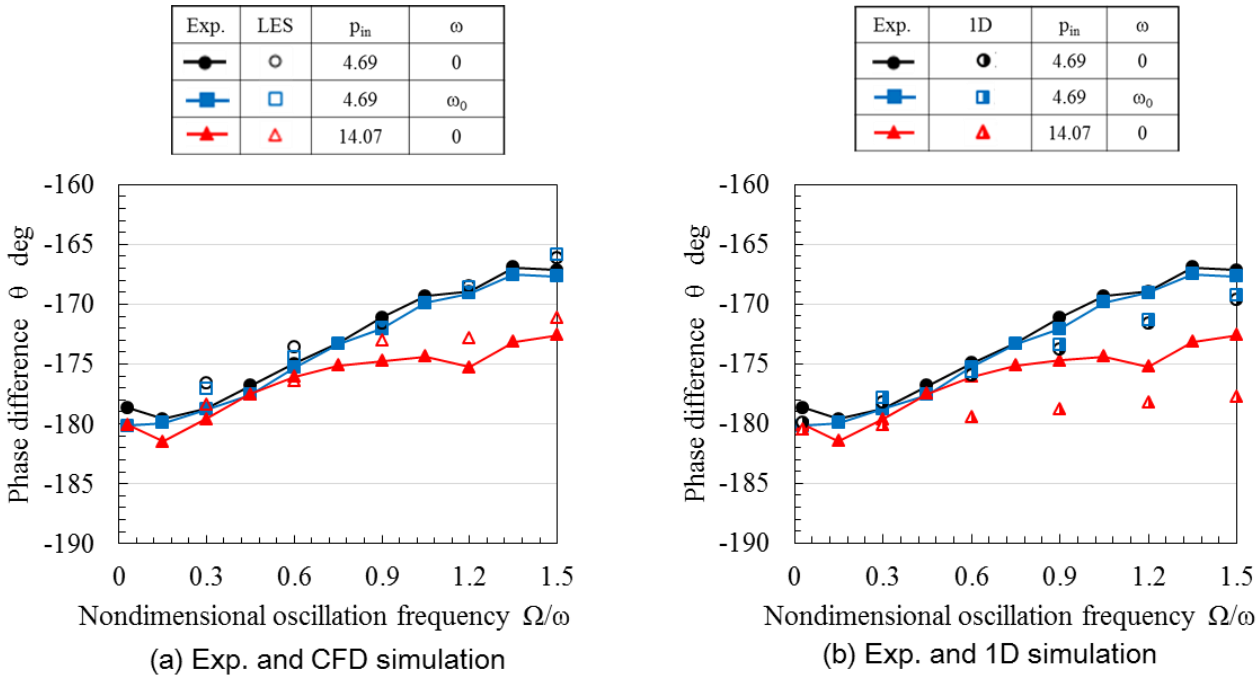

(a) Exp. and CFD simulation (b) Exp. and 1D simulation

Fig. 8 The phase difference θ

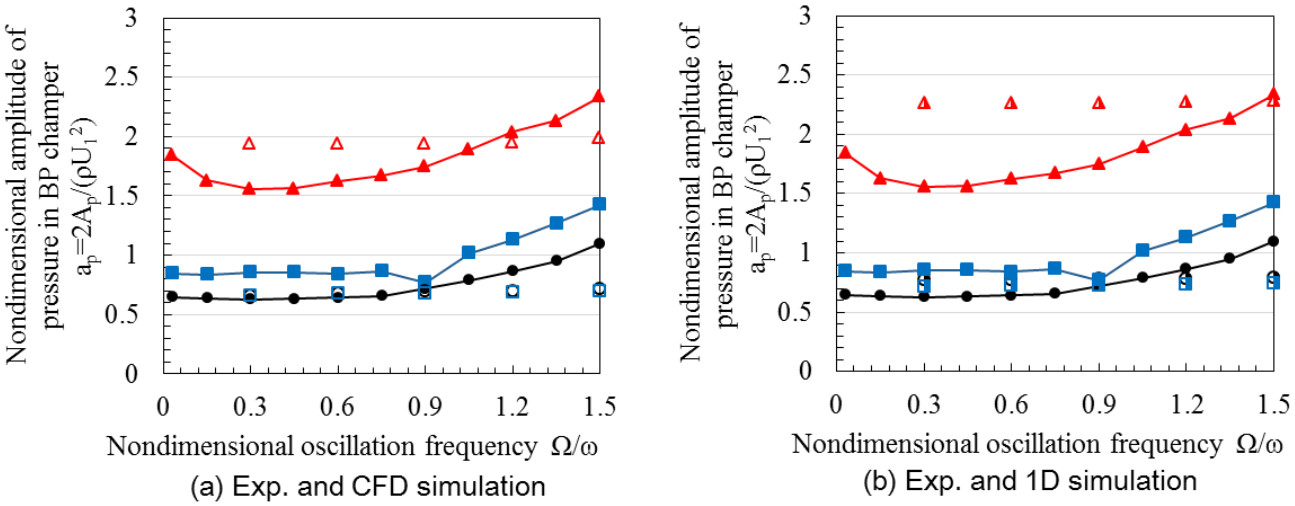

(a) Exp. and CFD simulation (b) Exp. and 1D simulation

Fig. 9 The amplitude of the static pressure fluctuation in BP chamber a_p

Fourier transform (FFT) analysis to calculate the frequency response of the phase difference from the rotor axial displacement to the static pressure fluctuation in the balance piston chamber and amplitude of the static pressure in the balance piston chamber.

The sine waveform of the static pressure in the balance piston chamber is shown in Eq. (3).

$$P_{BP} = A_p \sin(\Omega t + \theta) \qquad (3)$$

And, fluid force in the balance piston chamber is shown in Eq. (4).

$$\mathrm{F} = P_{BP} \cdot S = -M\ddot{X} - C\dot{X} - KX \qquad (4)$$

When the working fluid is air, and the added mass of the fluid is extremely small, we assumed that the added mass M is zero. Then, by substituting Eq. (1) and (3) to Eq. (4) and arranging these equations, the damping coefficient C and stiffness coefficient K are defined as follows.

$$\mathrm{C} = -\frac{A_p \sin\theta}{2\pi f A_x} S \qquad (5)$$

$$\mathrm{K} = -\frac{A_p \cos\theta}{A_x} S \qquad (6)$$

A positive or negative damping coefficient is determined by the phase difference from the rotor axial displacement to the static pressure fluctuation in the balance piston chamber. Therefore, when -180 $< \theta <$ 0 [deg], the damping coefficient is positive, and the balance piston is stable. On the other hand, when -360 $< \theta <$ -180 [deg], the damping coefficient is negative, and the balance piston is unstable.

Fig. 8 shows the phase difference from the rotor axial displacement to the static pressure fluctuation in the balance piston chamber obtained by the experiment, CFD, and 1D simulation results. The phase difference of the balance piston that was used in this study is primarily $-180 < \theta < 0$ [deg] and therefore, the damping coefficient is positive. And, Fig. 9 shows the amplitude of the static pressure in the balance piston chamber obtained by the experiment, CFD, and 1D simulation results.

2.2.1 Verification of the results of the simulations

From Fig. 8(a), the values of the phase difference of the experiment are in agreement with those of the CFD simulation. However, from Fig. 8(b), the values of phase difference at the same Ω/ω_0 differ slightly for the experiment and 1D simulation. For example, for the condition p_{in} =14.07, the phase difference approaches -173 [deg] (Experiment), -172 [deg] (CFD simulation), and -178 [deg] (1D simulation) at Ω/ω_0 = 1.5. Therefore, it is considered that the CFD simulation can be used to effectively predict the phase differences. On the other hand, the phase difference of the 1D simulation at Ω/ω_0 = 1.5 is about 5 [deg] smaller than that of the experiment and CFD simulation, and this difference cannot be ignored.

Considering the difference in the results obtained for the experiment and simulations, the results of the experiment and CFD simulation include the effects of three-dimensional (3D) flow and the shapes of the balance piston. However, that of the 1D simulation includes only the 1D characteristics and ignores the 3D effects. Therefore, it is believed that the difference in the phase difference between the experiment and 1D simulation is because the 1D simulation lacks the effects of 3D flow and shapes of the balance piston. In other words, this result implies that the 3D flow structure (vortex, etc.) and the shapes of the balance piston affect the fluctuation in the phase difference and dynamic characteristics.

From Fig. 9, although there are variations in the plots, the amplitude of the experiment is almost the same values as that of the simulations.

2.2.2 Effects of Rotating Speed

First, we examined the effect of the presence or absence of rotation on the dynamic characteristics of the balance piston for the condition where the upstream pressure of the No. 1 orifice p_{in} = 4.69 and the rotational speed $\omega = \omega_0$.The nominal No. 1 and No. 2 orifice clearances are $x_1/(x_1+x_2)$ = $x_2/(x_1+x_2)$ = 0.5.

At Ω/ω_0 = 0, when the rotor axial displacement is positive (the direction in which the No. 1 orifice clearance becomes smaller), the pressure loss in the No. 1 orifice becomes larger and the static pressure in the balance piston chamber decreases. Thus, the phase difference at Ω/ω_0 = 0 is -180 [deg]. From Fig. 8 and Fig. 9, regardless of the rotation, the phase difference θ of the experiment has a tendency to approach -166 [deg] at Ω/ω_0 = 1.5, and the pressure amplitude a_p has almost the same value. Therefore, for this condition ($\omega = \omega_0$), the effect of the disk rotation on the balance piston dynamic characteristics is extremely small. This tendency is almost the same as in the CFD and 1D simulations.

2.2.3 Effects of Upstream Pressure

Next, we examined the effect of the upstream pressure of the No. 1 orifice p_{in} for the condition where the $x_1/(x_1+x_2)$ = $x_2/(x_1+x_2)$ = 0.5 and the rotational speed ω = 0. The upstream pressure of the No. 1 orifice p_{in} was 4.69 and 14.07.

From Fig. 8 and Fig. 9, the phase difference of the experiment for the condition p_{in} = 4.69 approaches -166 [deg] at Ω/ω_0 = 1.5, and that for the condition p_{in} = 14.07 approaches -173 [deg]. The phase difference in the former case is a little larger than that in the latter case, and this trend was also observed in the CFD and 1D simulations. From these results, it is found that the condition p_{in} = 4.69 is more stable than the condition p_{in} = 14.07.

3 Conclusion

To examine the characteristics of the balance piston, we performed experiment and CFD, 1D simulations, and the results can be summarized as follows.

(1) To study the static characteristics of the balance piston, we calculated the pressure in the balance piston chamber and the flowrate curve and orifice flow coefficient. The characteristics of the experiment were almost the same as those in the CFD and 1D simulations.

(2) We calculated the magnitude and phase difference of the static pressure in the balance piston chamber. The characteristics of the experiment were almost same as those in the CFD simulation, but the phase difference in the 1D simulation was smaller than that of the experiment. Therefore, it is considered that the CFD simulation can be used to effectively predict the dynamic characteristics and stability of balance piston. And, there is a possibility that the 3D flow structure and

the shapes of the balance piston affect the fluctuation in the dynamic characteristics.

(3) We examined the effects of the rotational speed and upstream pressure of the No. 1 orifice on the balance piston dynamic characteristics, and it was found that the dynamic characteristics were dependent on the upstream pressure of the No. 1 orifice.

NOMENCLATURE

a_p	nondimensional amplitude of pressure in balance piston chamber $= 2A_p/\rho {U_1}^2$
a_x	nondimensional amplitude of axial oscillation of rotor $=A_x/(x_1+x_2)$
A_p	amplitude of pressure in balance piston chamber P_{BP} [Pa]
A_x	amplitude of axial oscillation of rotor [m]
c	nondimensional damping coefficient
C	damping coefficient [N/(m/s)]
f	frequency of axial oscillation of rotor [Hz] =Ω/(2π)
F	fluid force in the balance piston chamber [N]
k	nondimensional stiffness coefficient
K	stiffness coefficient [N/m]
M	added mass [kg]
R	diameter [m]
p	nondimensional static pressure $=2P/\rho {r_0}^2 {\omega_0}^2$
P	static pressure [Pa]
ΔP	rotational loss [Pa] , Eq. (2)
q	nondimensional flow rate $=Q/2\pi\omega_0 {r_0}^3$
Q	flow rate [m3/s]
r	radius [m]
S	disk area [m^2] $=\pi {R_1}^2 - \pi {R_2}^2$
U_1	tip speed of the rotating disk [m/s] $=r_1\omega_0$
x	orifice clearance [m]
X	axial displacement of rotor [m]
α	swirl ratio
ρ	air density [kg/m3]
θ	phase difference from axial displacement x to pressure in BP chamber P_{BP} [deg]
ω	rotational angular velocity [rad/s], ω_0=209.4
Ω	angular velocity of the axial oscillation of rotor [rad/s]

Subscript

0	nominal
1, 2	No.1 orifice and No.2 orifice of balance piston, respectively
in	No.1 orifice upstream
out	No.2 orifice downstream
BP	balance piston chamber

REFERENCES

[1] Kawasaki, S., Shimura, Uchiumi, M., T., Hayashi, M. and Matsui, J, 2011, “Unsteady Response of Flow System around Balance Piston in a Rocket Pump”, EUCASS-4.

[2] Childs, D. W., 1991, “Fluid-Structure Interaction Forces at Pump-Impeller-Shroud Surfaces for Axial Vibration Analysis”, Journal of Vibration and Acoustics, vol. 113.

[3] Horiguchi, H., Ueno, Y., Takahashi, K., Miyagawa, K. and Tsujimoto, Y., “Dynamic Characteristics of the Radial Clearance Flow between Axially Oscillating Rotational Disk and Stationary Disk”, International Journal of. Fluid Machinery and Systems, Vol. 2, No.2 (2009), pp.147-155.

[4] Shimura, T., Kawasaki, S., Uchiumi, M., Kimura, T. and Matsui, J, 2012, “Internal Flow and Axial Thrust Balancing of a Rocket Pump”, Journal of Fluid Engineering, vol.134, 041103-1.

[5] Shimura, T., Kawasaki, S., Uchiumi, M., Kimura, T., Hayashi, M. and Matsui, J, 2012, “Dynamic Response on an Axial Thrust Balancing System for Rocket Pumps”, ISROMAC-14.

[6] Kawasaki, S., Kimura, T., Uchiumi, M., Shimura, T., Hayashi, M. and Matsui, J, 2012, “Numerical Investigation of Axial Force Dynamics on Balance Piston of a Rocket Pump”, ISROMAC-14.

[7] Shimura, T., Kawasaki, S., Uchiumi, M., Kimura, T. Hayashi, M. and Matsui, J, 2013, “Stability of an Axial Thrust Self-Balancing System”, Journal of Fluid Engineering, vol.135, 011105-1.

[8] http://www.cradlecfd.com/products/sctetra/index.html (2015)

[9]http://www.plm.automation.siemens.com/en_us/products/lms/imagine-lab/amesim/ (2015)